CrossMark

ORIGINAL ARTICLE

InSAR-derived digital elevation models for terrain change analysis of earthquake-triggered flow-like landslides based on ALOS/PALSAR imagery

Yu Huang · Miao Yu · Qiang Xu · Kazuhide Sawada · Shuji Moriguchi · Atsushi Yashima · Chengwei Liu · Long Xue

Abstract Earthquakes can directly trigger multiple simultaneous slope failures in mountainous regions. Among these slope failures, flow-like landslides with high velocities and long run-outs can result in damage that is more destructive than other types of landslides. Timely and accurate recognition of the locations and magnitudes of flow-like landslides is essential for post-disaster relief. Synthetic aperture radar (SAR) sensors are suitable for deformation monitoring because of their capability to operate at day or night and in all weather conditions. Interferometric synthetic aperture radar (InSAR) is an advanced technique that extracts three-dimensional terrain and changes information from the radar images at a regional scale. The focus of this study is the Donghekou landslide-debris flow that was triggered by the 2008 Wenchuan earthquake. ALOS/PALSAR remote satellite images were interpreted by InSAR to generate digital surface elevation models. A comparison of data from a typical InSAR configuration with field survey data proves that the former is an effective method for rapidly detecting flow-like landslides in a mountainous area. The comparison also shows that the accuracy of the results is closely related to the correlation between the satellite radar images used, and further that the study accuracy would improve with the inclusion of better correlation. In this way, representations of pre- and post-landslide terrains could be generated for use in numerical simulations. The InSAR method has particular significance for areas without terrain data prior to slope failure, and can provide basic data for landslide hazard assessments.

Y. Huang (✉) · M. Yu · C. Liu · L. Xue
Department of Geotechnical Engineering, College of Civil Engineering, Tongji University, Shanghai 200092, China
e-mail: yhuang@tongji.edu.cn

Y. Huang
Key Laboratory of Geotechnical and Underground Engineering of the Ministry of Education, Tongji University, Shanghai 200092, China

Q. Xu
State Key Laboratory of Geo-hazard Prevention and Geo-environment Protection, Chengdu University of Technology, Chengdu 610059, China

K. Sawada · A. Yashima
Department of Civil Engineering, Gifu University, Gifu 501-1193, Japan

S. Moriguchi
International Research Institute of Disaster Science, Tohoku University, Sendai 980-8579, Japan

Introduction

Earthquake-triggered flow-like landslides commonly slide over long distances (from a few hundred meters to several kilometers) at high speeds (on the order of meters per second) (Hungr et al. 2001; Huang et al. 2012; Huang and Dai 2014). Flow-like landslides can include debris flows, debris avalanches, flow slides, rock avalanches, and earth flows. Because of the extent of the affected area and the short evacuation time, a flow-like landslide can result in more serious damage than other types of landslide. For example, the 1949 seismically induced Khait flowslide that extended 7.41 km with a volume of 75×10^6 m^3 at an average speed of ~ 30 m/s caused around 800 deaths (Evans et al. 2009). The Las Colinas flow-like landslide,

Springer

triggered by the 2001 El Salvador earthquake, slid 800 m with a huge volume of 183,500 m^3 and killed 485 people (Crosta et al. 2005).

Rapid detection of the location and boundaries of flow-like landslides following earthquakes is crucial for post-disaster relief and reconstruction. Conventional field investigations have many deficiencies. (1) Some are not suitable for regional scale surveys because of the large amount of time and the extent of financial resource consumption required to produce precise results (Peyret et al. 2008). (2) Other conventional methods are rarely conducted in mountainous terrain because of the lack of accessibility to landslide regions during and after earthquakes. (3) Additionally, field surveys cannot recover original terrain surfaces before the landslide occurrence (Gong et al. 2010). For that matter, even topographic data from rugged mountainous areas in many developing countries may not be available prior to a geohazard event.

Over the last few decades, remote sensing technology has been widely used in geohazard investigations and assessments. For example, Abdikan et al. (2014) monitored the coal mining subsidence and proved the usefulness of Phased Array Type L-band Synthetic Aperture Radar data (PALSAR) in avoiding signal decorrelation and deformation detection in the heavily vegetated areas. Zhou et al. (2014) monitored the movement of mountain glaciers with velocity scale of m/year by InSAR and obtained the factors influencing glacier velocity through quantitative analysis. Pardo et al. (2013) applied InSAR technique to quantitative analysis of the historical land surface deformation, and the results can calibrate finite elements deformation. Gupta et al. (2014) used InSAR technique to monitor elevation changes in Jharia coalfield (India) and put forward that high vertical accuracy is difficult to be obtained in surface deformation studies. Dong et al. (2014) measured ground subsidence associated with rapid urbanization in Shanghai (China) by Small Baseline Subset (SBAS) InSAR method and the approximate deformation rate is 0.5–3 cm/year. The authors suggest that multi-track SAR data (descending and ascending) should be combined in a future study to obtain both vertical and horizontal deformations.

Landslide is one of the main types of geological disasters. For landslide monitoring studies, the InSAR technique has gained increasing significance, for example: (1) in landslide detection and inventory at regional scales (Catani et al. 2005; Singh et al. 2005; Zhao et al. 2012; Wang et al. 2013), and (2) in monitoring deformation of individual landslides (e.g., Strozzi et al. 2005; Zhang et al. 2013; Greif and Vlcko 2012; Peyret et al. 2008; Liu et al. 2013).

Previous studies mainly focused on long-term monitoring of small deformation, but relatively a small number of studies concentrate on sudden slope failure triggered by earthquakes. In this study, L-band ALOS/PALSAR remote satellite images are interpreted by the InSAR technique to generate digital surface elevation models before and after a given landslide. The Donghekou landslide-debris flow, triggered by the 2008 Wenchuan earthquake, is the focus of this study. The locations and boundaries of such flow-like landslides can be determined rapidly by subtracting a digital elevation model (DEM) constructed before the landslide from the one constructed after the landslide. By comparing typical pre- and post-failure configurations with field survey data, the accuracy of InSAR results is enough for further risk assessment of flow-like landslides. In addition, this method can effectively overcome field survey limitations, such as massive time consumption, incapability in the inaccessibility area. Hence, the InSAR technique has proved to be an effective method for the rapid detection of flow-like landslides and can provide a reference for risk assessments of flow-like landslides.

InSAR technology and ALOS/PALSAR images

InSAR technology

InSAR, a microwave remote sensing technology, can generate a regional DEM from paired satellite radar images by calculating the phase difference between the images. The accuracy of the method theoretically can reach meter-scale resolution if accurate satellite data can be acquired (Yin et al. 2010). Sources of error in the results can include atmospheric phase distortions, orbital error, signal noise, look angle error, phase unwrapping mistakes, and edge effects in the SAR images (Strozzi et al. 2005).

In this study, the InSAR process involved six main steps. (1) Co-registration is the first interference step, and it directly affects the accuracy of the DEM. Registration accuracy should reach 0.1 pixels through interpolation processing of the original images. (2) An interference image is generated through a process of conjugate correspondence between points in the two complex images. (3) A filtering process was undertaken to eliminate noise generated during data acquisition and the subsequent data processes. To a large extent, an appropriate filtering method can remove noise and maintain the continuity of the interference fringes. In this study, Goldstein filtering method and convolution filtering method were used. Both methods can remove noises effectively. But convolution filtering method would also dispose some useful topographical information simultaneously. Hence, the Goldstein filtering method can better meet the requirements. (4) Flat earth effects refer to cyclical changes of interferometric phase caused by flat ground that, to some extent, obscure interference fringe changes induced by terrain deformation. In this study, the SRTM DEM with a

resolution of 90 m was used to remove the flat earth effect. (5) Phase unwrapping is a process that restores the interferometric phase to true phase. In this study, minimum cost flow algorithms was used, and the results fit well with SRTM DEM. (6) The elevations of ground points were obtained by calculating the geometrical relationship between phase and elevation. Then, the DEM derived from SAR data was integrated with SPOT optical images, so that the landslide damages can be better understood.

ALOS/PALSAR images

The Advanced Land Observing Satellite (ALOS) was successfully launched by the Japan Aerospace Exploration Agency on 24 January 2006. It is equipped with two optical sensors and one synthetic aperture radar sensor used for cartography and disaster monitoring of Asia and the Pacific. ALOS was launched on a sun-synchronous orbit at an elevation of 691.65 km with a revisit period of 46 days. Additionally, the ALOS satellite has the flexibility to adjust its orbit in response to natural hazard emergencies.

The SAR sensor, PALSAR, is an active microwave sensor that provides a day-and-night and all weather acquisition capability in its collection of surface change information. PALSAR has five observation modes (Shimada et al. 2008): (1) fine-beam single (FBS): with single polarization of HH or VV, and 10-m resolution, (2) fine-beam dual: with dual polarization of HH + HV or VV + VH, and 20-m resolution, (3) ScanSAR mode: with 100-m resolution, (4) full polarimetry mode (POL): with 30-m spatial resolution, and (5) direct transmission (DT) mode: with single polarization. The FBS mode data were used in this study because of its high resolution.

There are three reasons why the ALOS/PALSAR data were used as the basis for this study. (1) In 2008, the year of the Wenchuan earthquake, ALOS was quite advanced in comparison with contemporaneous, high-resolution cost-effective civilian satellites. (2) Since 2007, PALSAR data cover was already available for the entire land area of China. (3) Compared with C-band (5.3 GHz, 5.7-cm wavelength) images, L-band (1.3 GHz, 23.5-cm wavelength) images are more suitable for detecting rapid displacement in vegetated area, because the longer wavelength has the ability to reduce intrinsic ambiguity of phase measurements and penetration capacity in the vegetation canopy (Strozzi et al. 2005).

Case study of Donghekou landslide-debris flow

Study area

On 12 May 2008 at 14:28 CST, the devastating Wenchuan earthquake (M_s 8.0; M_w 7.9), triggered by the motion of the Longmenshan fault, occurred with an epicenter in Yingxiu Town, Wenchuan County, Sichuan Province, China. It induced surface ruptures approximately 300 km long with extensive damage over an area of 130,000 km^2 (Huang and Li 2009). There were 54,971 aftershocks cataloged, with the largest one having a magnitude of M_s 6.4 on 27 May 2009. The geological environment of the impacted mountainous area had already been extremely vulnerable before the earthquake because of the long-term impact of tectonic movements. Hence, the strong long-duration seismic shaking resulting from the earthquake and acting on the unstable slopes resulted in landslide damage that was even more catastrophic than that caused by the earthquake itself (Zhou et al. 2013).

The Donghekou landslide-debris flow is typical flow-like landslides induced by the 2008 Wenchuan earthquake. The central coordinate of the Donghekou landslide-debris flow is N 32°24′31″, E 105°06′40″. It occurred at the confluence of the Qingzhujiang and Hongshihe rivers, about 225 km away from the epicenter. The slide mass was primarily composed of dolomite and siliceous limestone of the Sinian system, along with Cambrian carbonaceous slate and phyllite (Sun et al. 2011). For more details of the geological map of study area please refer to the Fig. 1 in Dai et al. (2011), and the Donghekou debris flow is located in the Qingchuan County, the upper right corner of the figure.

The crown elevation of the landslide is about 1,300 m and the height difference between the crown and the toe is about 600 m. The slide ran out approximately 2,400 m, involving a huge volume of around 10×10^6 m^3 that formed three large landslide dams (Yin et al. 2009). The river may have contributed to the high speed and long runout by inducing undrained behavior during the movement (Wang et al. 2009). Figure 1a shows an aerial view of the landslide based on Google Earth data.

The failure process can be classified into three parts. First, cracks appeared on the slopes under strong seismic loading and slope failure was triggered with an initial velocity. Then, with the increasing sliding speed, the landslide mass was crushed due to collisions and advanced over a long distance at high speeds. Finally, the velocity of the slide decreased when reaching a small slope angle, and came to a stop (Zhou et al. 2013).

The slide caused serious damage; four villages were buried, and at least 300 deaths occurred. Therefore, a study involving this type of landslide is of significant social and scientific value, and could provide a basis for risk analysis assessments of similar cases in the future. Additionally, field data collected before and after the Donghekou landslide are both available and, therefore, can be used to provide a validation of the InSAR technique.
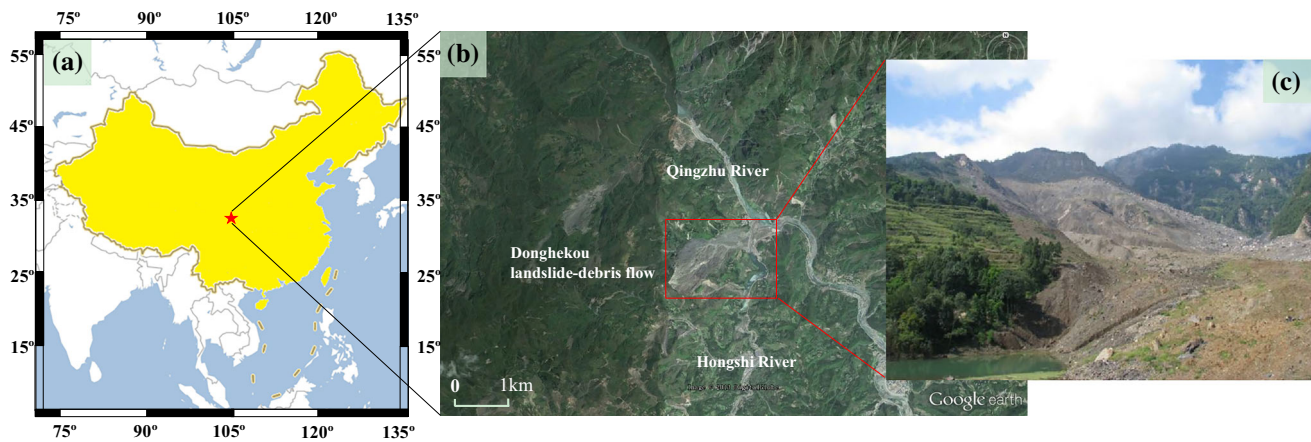
Fig. 1 Donghekou landslide-debris flow. **a** Location of Donghekou landslide-debris flow in China. **b** Aerial view of the landslide based on Google Earth data. **c** Photo of Donghekou landslide-debris flow

Table 1 ALOS PALSAR image list

Number	Image number	Data mode	Frame	Perpendicular baselines (m)	Acquisition data
1	ALPSRP100880630	FBS	630	267.14	2007/12/16
2	ALPSRP107590630	FBS	630		2008/01/31
3	ALPSRP154560630	FBS	630	568.75	2008/12/18
4	ALPSRP161270630	FBS	630		2009/02/18

In this study, two pairs of L-band ALOS/PALSAR images with 10-m spatial resolution were used. Table 1 shows the data mode, frame, baseline distance, and acquisition data for the images.

Field investigation

3D terrain data of Donghekou debris flow after the Wenchuan earthquake were acquired by an advanced three-dimensional laser scanning from the Chengdu University of Technology. The scanning system is called Intelligent Laser Ranging and Imaging System (ILRIS-3D) developed by Optech Incorporated, Ontario, Canada. By calculating the fight time of laser pulse from the emission to the return, the distance of a reflecting object can be obtained. The accuracy of scanning results can achieve ±8 (mm 100 m). Table 2 lists the working parameters of the ILRIS-3D (Huang et al. 2014).

In addition, the terrain data prior to the earthquake were derived by interpreting the 1:50,000 topographic map of Qingchuan County.

Analysis of InSAR results from ALOS PALSAR images

Interferometric coherence is a measure of correlation between two SAR images, which determines whether the

Table 2 Working parameters of ILRIS-3D (Huang et al. 2014)

Model	ILRIS 3D
Manufacturer	Optech
Scanning distance (m)	3–1,000
Accuracy/mm (100 m)$^{-1}$	±8
Scan trace	40° × 40°
Data sampling rate (dot s^{-1})	2,000
Wave length of laser (nm)	1,500
Laser level	Class 1
Dimensions (cm^3)	320 × 320 × 220
Machine mass (kg)	13
Voltage (V)	24
Software	Polyworks 8.0
RGB function	Yes

interferometric phase can reflect the surface elevation reliably. The value of coherence magnitude ranges from 0 to 1. The larger value represents the higher coherence. The interferometric coherence of pre- and post-landslide images was calculated as shown in Fig. 2. The coherence of post-landslide image was much better, mostly >0.5, while the coherence of pre-landslide image was mostly between 0.3 and 0.6. Because of this, pre-landslide DEM contains more speckle noise, as shown in Fig. 3. The grid size of the DEMs is 15 m. Most error in the models occurred in valleys and along ridges in the mountainous environment

Fig. 2 Image coherence pre-
and post-landslide. *Red
rectangle* indicates the region
of the Donghekou landslide-debris
flow

(a) Coherence pre-landslide   **(b)** Coherence post-landslide
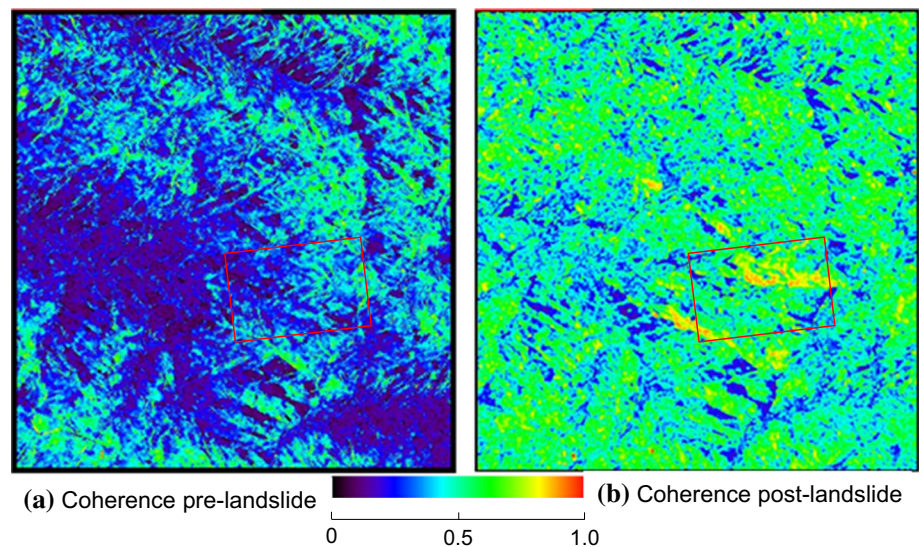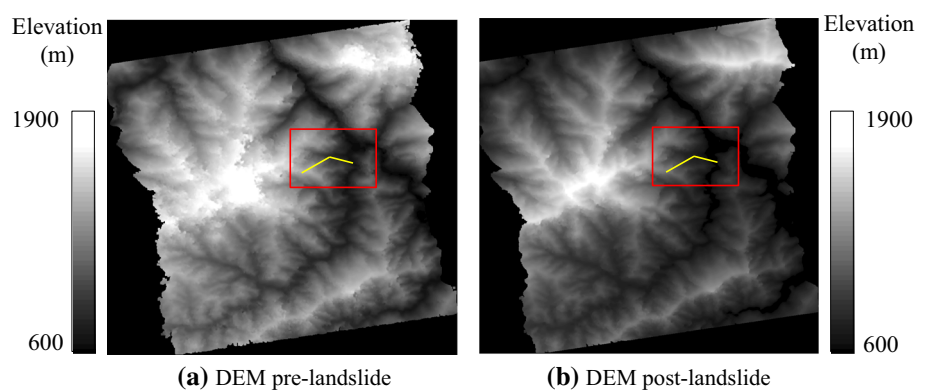
0   0.5   1.0

Fig. 3 Pre- and post-landslide
DEMs extracted from ALOS by
InSAR. *Red rectangle* indicates
the region of the Donghekou
landslide-debris flow. *Yellow
line* presents the typical profile

Elevation (m)

1900

600

(a) DEM pre-landslide

Elevation (m)

1900

600

(b) DEM post-landslide

because of the low coherence induced by layover and shadow effects (Singh et al. 2005).

By integrating the DEM derived from SAR images with SPOT optical images, a three-dimensional model of the Donghekou landslide-debris flow can be obtained. Such a model is helpful for recognizing the location and range of slope failures, as shown in Fig. 4. The total volume of the landslide is estimated to be approximately 41×10^6 m³ by subtracting the pre-landslide DEM from the post-landslide model. Figure 5 represents elevation difference of InSAR DEMs pre- and post-landslide, which is helpful for better understanding of the locations of volume changes. The area marked by red line is the sliding source and traveling area, the value of which is negative, while the zone marked by blue dotted line presents the deposition area, the value of which is positive.

In Fig. 6, the slide distance of the Donghekou landslide-debris flow was around 2.1 km; it can be divided into three parts: a sliding source, a traveling area, and a deposition area. The landslide started at an elevation of around 1,300 m and formed a steep slope with a height of around 80 m and a dip angle of around 70°. Downhill, the slope angle decreased to a value of about 20°.

Elevation error analyses

The elevation errors of the InSAR DEMs pre- and post-landslide were analyzed by comparing them with laser scan results and 1:50,000 topographic map, respectively. The mean elevation error prior to landslide is 37.5 m, while that posterior to landslide is 33.1 m.

The root-mean-square (RMS) errors in vertical accuracy pre- and post-failure are 40.34 and 46.63 m, respectively. However, the InSAR result post-failure is very similar to the landslide configuration determined from survey data within a range of 1,000 m. The RMS error of 0–1,000 m is 28.61 m, while that of 1,000–2,100 m is 58.53 m. The main reason for the huge error of 1,000–2100 m is that the acquisition times were different for the field survey and satellite images. The Donghekou landslide formed three landslide dams. A typical profile can be observed crossing the Hongshihe landslide dam. The height, length, and width
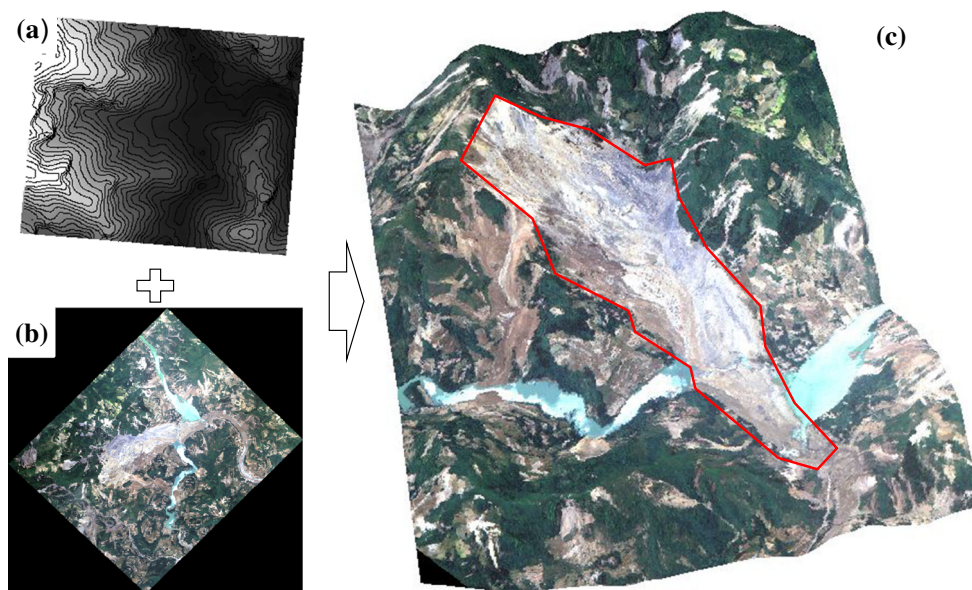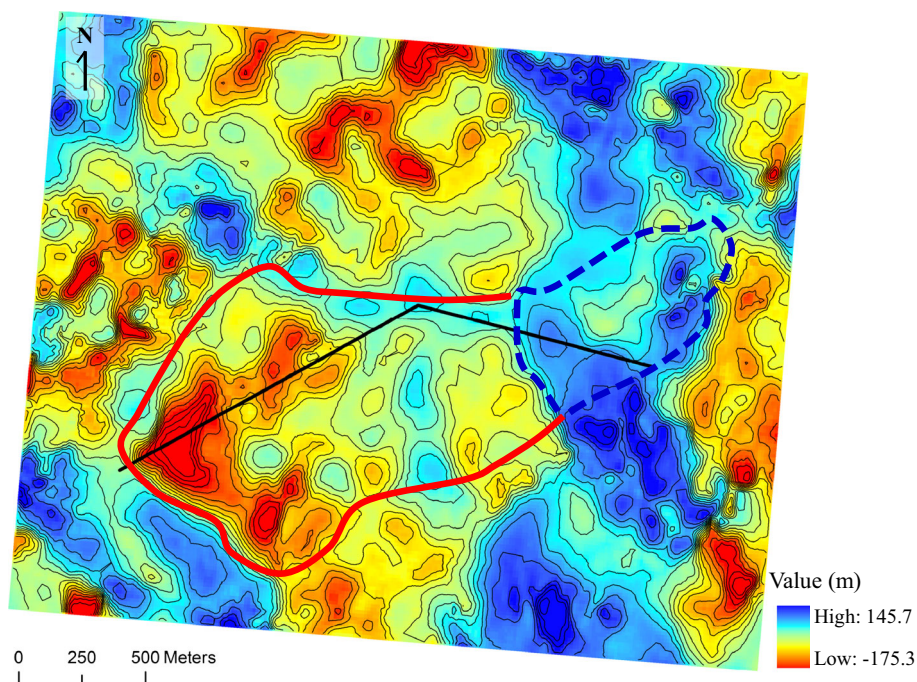
Fig. 4 Donghekou landslide-debris flow. **a** DEM post-landslide (*red rectangle* in Fig. 3b). **b** SPOT image post-landslide. **c** Three-dimensional modeling

Fig. 5 Elevation difference of InSAR DEMs pre- and post-landslide

of the Hongshihe landslide dam were approximately 50, 500, and 250 m, respectively, and the reservoir volume is roughly 4×10^6 m^3 (Chang et al. 2011). Because the risk of an outburst flood induced by the failure of Hongshihe landslide dam is quite high, emergency measures were taken immediately after the earthquake involving an excavation design volume exceeding 50,000 m^3 (Ren and Dang 2008).

Compared with the post-failure error, the RMS error of pre-failure in the range of 0–1,000 m is larger with a

value of 39.36 m. Overall, the accuracy of the post-landslide DEM is superior to the pre-landslide DEM in the range of 0–1000 m, and it can be concluded that the accuracy of the modeling results is closely related to the coherence of the satellite radar images. Accuracy of results will be improved if the coherence of pre-landslide images can be improved. The method presented here is especially significant for areas without pre-landslide terrain data, and can provide basic data for landslide hazard assessment.
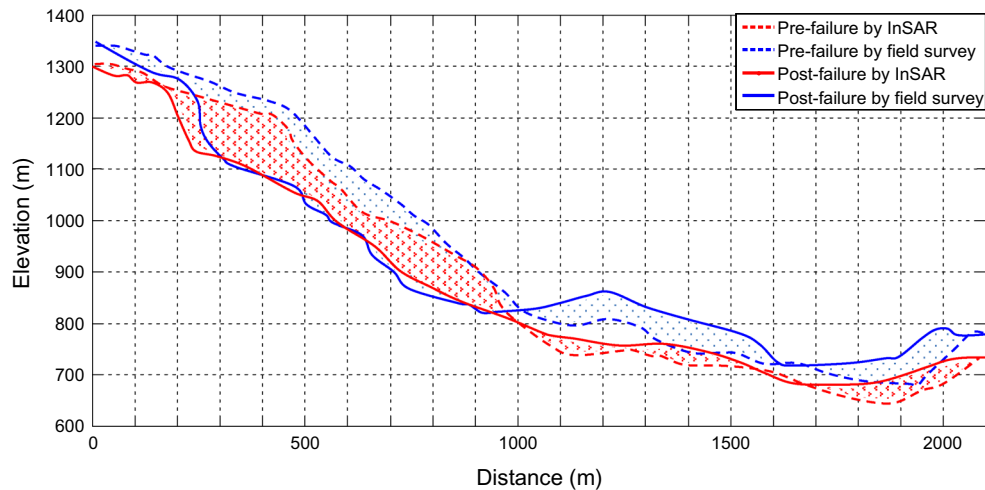
Fig. 6 Pre- and post-failure profile derived by InSAR and field surveying for the Donghekou landslide-debris flow

Conclusions

Flow-like landslides with high velocities and long run-outs can result in more destructive damage than other types of landslides. Recognition of the locations and magnitudes of flow-like landslides is essential for post-disaster relief. InSAR is an emerging technique that can be used to measure wide-scale regional terrain deformation efficiently.

In this study, the well-known Donghekou landslide-debris flow triggered by the 2008 Wenchuan earthquake was used to verify the feasibility of the InSAR technique for detecting rapidly moving landslides. ALOS/PALSAR remote satellite images were interpreted by the InSAR method to generate digital surface elevation models before and after the landslide; typically configured InSAR results fit well with survey data collected in the field. By subtracting the pre-landslide DEM from after the post-landslide DEM, the location and volume of the landslide can be determined. Through comparison, the interference coherence of SAR image pair is important for the result accuracy. This method provides a way to regenerate the terrain configuration before a landslide, which can then be used for numerical simulations. This is of particular significance for areas without original terrain data prior to slope failure, and provides basic data required for landslide hazard assessments.

References

Abdikan S, Arıkan M, Sanli FB, Cakir Z (2014) Monitoring of coal mining subsidence in peri-urban area of Zonguldak city (NW Turkey) with persistent scatterer interferometry using ALOS-PALSAR. Environ Earth Sci 71(9):4081–4089

Catani F, Casagli N, Ermini L, Righini G, Menduni G (2005) Landslide hazard and risk mapping at catchment scale in the Arno river basin. Landslides 2(4):329–342

Chang DS, Zhang LM, Xu Y, Huang RQ (2011) Field testing of erodibility of two landslide dams triggered by the 12 May Wenchuan earthquake. Landslide 8(3):321–332

Crosta GB, Imposimato S, Roddeman D, Chiesa S, Moia F (2005) Small fast-moving flow-like landslides in volcanic deposits: the 2001 Las Colinas Landslide (El Salvador). Eng Geol 79(3–4):185–214

Dai FC, Xu C, Yao X, Xu L, Tu XB, Gong QM (2011) Spatial distribution of landslides triggered by the 2008 Ms 8.0 Wenchuan earthquake, China. J Asian Earth Sci 40(3):883–895

Dong SC, Samsonov S, Yin HW, Ye SJ, Cao YR (2014) Time-series analysis of subsidence associated with rapid urbanization in Shanghai, China measured with SBAS InSAR method. Environ Earth Sci 72(3):677–691

Evans SG, Roberts NJ, Ischuk A, Delaney KB, Morozova GS, Tutubalina O (2009) Landslides triggered by the 1949 Khait earthquake, Tajikistan, and associated loss of life. Eng Geol 109(3–4):195–212

Greif V, Vlcko J (2012) Monitoring of post-failure landslide deformation by the PS-InSAR technique at Lubietova in Central Slovakia. Environ Earth Sci 66(6):1585–1595

Gupta M, Mohanty KK, Kumar D, Banerjee R (2014) Monitoring surface elevation changes in Jharia coalfield, India using synthetic aperture radar interferometry. Environ Earth Sci 71(6):2875–2883

Gong JH, Wang DC, Li Y, Zhang LH, Yue YJ, Zhou JP, Song YQ (2010) Earthquake-induced geological hazards detection under hierarchical stripping classification framework in the Beichuan area. Landslides 7(2):181–189

Huang Y, Dai ZL (2014) Large deformation and failure simulations for geo-disasters using smoothed particle hydrodynamics method. Eng Geol 168:86–97

Huang Y, Dai ZL, Zhang WJ (2014) Geo-disaster modeling and analysis: an SPH-based approach. Springer, Heidelberg, pp 184–185

Huang Y, Zhang WJ, Xu Q, Xie P, Hao L (2012) Run-out analysis of flow-like landslides triggered by the Ms 8.0 2008 Wenchuan earthquake using smoothed particle hydrodynamics. Landslides 9(2):275–283

Huang RQ, Li WL (2009) Development and distribution of geohazards triggered by the 5.12 Wenchuan earthquake in China. Sci China Ser E-Technol Sci 52(4):810–819

Hungr O, Evans SG, Bovis MJ, Hutchinson JN (2001) A review of the classification of landslides of the flow type. Environ Eng Geosci 7(3):221–238

Liu P, Li ZH, Hoey T, Kincal C, Zhang JF, Zeng QM, Muller JP (2013) Using advanced InSAR time series techniques to monitor landslide movements in Badong of the three Gorges region, China. Int J Appl Earth Obs Geoinf 21:253–264

Pardo JM, Lozano A, Herrera G, Mulas J, Rodriguez A (2013) Instrumental monitoring of the subsidence due to groundwater withdrawal in the city of Murcia (Spain). Environ Earth Sci 70(5):1957–1963

Peyret M, Djamour Y, Rizza M, Ritz JF, Hurtrez JE, Goudarzi MA, Nankali H, Chéry J, Dortz KL, Uri F (2008) Monitoring of the large slow Kahrod landslide in Alborz mountain range (Iran) by GPS and SAR interferometry. Eng Geol 100(3–4):131–141

Ren X, Dang XP (2008) Construction organization and construction management for emergency risk-elimination of landslide dams in Qingchuan County. Chin J Water Resour Hydropower Eng 39(8):27–30 (In Chinese)

Shimada M, Ozawa T, Fukushima Y, Furuya M, Rosenqvist A (2008) Japanese L-band radar improves surface deformation monitoring. Eos, Trans Am Geophys Union 89(31):277–278

Singh LP, Van Westen CJ, Champati Ray PK, Pasquali P (2005) Accuracy assessment of InSAR derived input maps for landslide susceptibility analysis: a case study from the Swiss Alps. Landslides 2(3):221–228

Strozzi T, Farina P, Corsini A, Ambrosi C, Thuring M, Zilger J, Wiesmann A, Wegmuller Urs, Werner C (2005) Survey and monitoring of landslide displacements by means of L-band satellite SAR interferometry. Landslides 2(3):193–201

Sun P, Zhang YS, Shi JS, Chen LW (2011) Analysis on the dynamical process of Donghekou rockslide-debris flow triggered by 5.12 Wenchuan earthquake. J Mt Sci 8(2):140–148

Wang FW, Cheng QG, Highland L, Miyajima M, Wang HB, Yan CG (2009) Preliminary investigation of some large landslides triggered by the 2008 Wenchuan earthquake, Sichuan Province, China. Landslides 6(1):47–54

Wang GJ, Xie MW, Chai XQ, Wang LW, Dong CX (2013) D-InSAR-based landslide location and monitoring at Wudongde hydropower reservoir in China. Environ Earth Sci 69(8):2763–2777

Yin YP, Wang FW, Sun P (2009) Landslide hazards triggered by the 2008 Wenchuan earthquake, Sichuan, China. Landslides 6(2):139–151

Yin YP, Zheng W, Liu YP, Zhang JL, Li XC (2010) Integration of GPS with InSAR to monitoring of the Jiaju landslide in Sichuan, China. Landslides 7:359–365

Zhang DX, Wang GH, Yang TJ, Zhang MC, Chen SH, Zhang FY (2013) Satellite remote sensing-based detection of the deformation of a reservoir bank slope in Laxiwa Hydropower Station, China. Landslides 10(2):231–238

Zhao CY, Lu Z, Zhang Q, Fuente J (2012) Large-area landslide detection and monitoring with ALOS/PALSAR imagery data over Northern California and Southern Oregon, USA. Remote Sens Environ 124:348–359

Zhou JW, Cui P, Yang XG (2013) Dynamic process analysis for the initiation and movement of the Donghekou landslide-debris flow triggered by the Wenchuan earthquake. J Asian Earth Sci 76:70–84

Zhou JM, Li Z, Guo WQ (2014) Estimation and analysis of the surface velocity field of mountain glaciers in Muztag Ata using satellite SAR data. Environ Earth Sci 71(8):3581–3592